Relativistic Doppler frequency upconversion of terahertz pulses reflecting from a photoinduced plasma front in silicon

Fanqi Meng, Mark D. Thomson, and Hartmut G. Roskos*

Physikalisches Institut, J. W. Goethe-Universität, Max-von-Laue-Strasse 1, 60438 Frankfurt am Main, Germany

(Received 11 September 2014; revised manuscript received 6 October 2014; published 30 October 2014)

We demonstrate experimentally the frequency upconversion of a terahertz (THz) pulse by the relativistic Doppler reflection from a counterpropagating charge-carrier plasma front in high-resistivity Si. The plasma front is generated via interband excitation with an ultrashort optical pump pulse. Spectral components extending to ∼28 THz are observed, using an input THz pulse with a bandwidth of ∼20 THz obtained from a two-color gas plasma emitter. We model the experiment using one-dimensional finite-difference time-domain simulations with realistic values of the Drude parameters for the plasma front, including effects due to excitation from a weak prepulse structure on the pump pulse.

DOI: 10.1103/PhysRevB.90.155207 PACS number(s): 78.47.−p

I. INTRODUCTION

The reflection of radiation from a rapidly counterpropagating boundary leads to a frequency upshift due to the relativistic Doppler effect [1]. To achieve a significant upshift factor, the boundary must possess a velocity comparable with that of the incident light, as can be realized, e.g., via an accelerated electron beam [2] or from rapid motion of charges in a nonuniform plasma [3–7]. It was also realized [8,9] that the moving boundary does not have to involve longitudinal motion of the constituent material particles, i.e., one may also employ an ionization front, where the motion of the plasma discontinuity is due to a counterpropagating optical excitation pulse. The frequency upshift factor $\Gamma = \omega_r/\omega_i$ between the incident (ω_i) and reflected (ω_r) waves is ideally given by $\Gamma = (1+\beta)/(1-\beta)$, where $\beta = U/c$ in terms of the propagation speeds of the plasma front (U) and incident radiation c (in the medium [10]). For the incident wave to experience an appreciable (metallic) reflection, the plasma density N (and hence plasma frequency ω_p, where $\omega_p^2 = Ne^2/\epsilon_0\epsilon_r m$) must be high enough that the condition $\omega_p \geqslant \sqrt{\Gamma}\omega_i \equiv \omega_{cr}$ is fulfilled [9,10].

In particular, for use in the terahertz (THz) spectral range, we previously proposed and investigated theoretically the use of interband excitation of charge carriers in a solid-state medium with an ultrashort pump pulse to produce the plasma front [10], which, compared to the tunnel ionization of a gas medium [11], allows one to readily achieve the required plasma densities over a sufficiently large cross section with pump-pulse energies available from tabletop-scale femtosecond amplifier lasers. For broadband THz spectroscopy, the Doppler upshift could be used to increase the bandwidth of existing high-energy THz sources, such as those based on optical rectification in $LiNbO_3$ [12–14], or large-area surface emitters [15] (which are generally limited to a bandwidth of only a few THz). Moreover, the experimental geometry with counterpropagating optical excitation and THz probe pulses offers a novel geometry for the investigation of the plasma charge-carrier dynamics themselves [16]. As a separate optical pump pulse is used to generate the moving front, the interpretation of such experiments is more straightforward compared, e.g., to the self-induced frequency shift of optical pulses reflecting from a semiconductor with saturable absorption about an exciton transition [17,18], where more complex interband dynamics are both driven and probed by the same pulse.

We identified (high-resistivity) Si as a highly suitable medium for experiments with near-ir optical pump pulses, as it fulfills several criteria. First, the plasma-front velocity (equal to the group velocity of the pump pulse $U = v_{g,op}$) is lower than the THz phase velocity (c_{THz}), allowing the reflected THz pulse to escape the medium, while their ratio β yields a significant upshift factor (e.g., $\Gamma \sim 8$ for a pump wavelength $\lambda_{ex} = 800$ nm, neglecting pump depletion effects [10]). Moreover, Si possesses a very low dispersion/loss for the incident and reflected pulses over the whole THz range and well into the infrared. Finally, the moderate absorption coefficient α_{ex} (due to the indirect interband transition) results in a favorable compromise between the achievable plasma density and the pump depletion length $L_\alpha = \alpha_{ex}^{-1}$, and hence the time interval $t_\alpha = (\alpha_{ex} v_{g,op})^{-1}$ over which the plasma front penetrates into the medium is suitably long for interaction with input broadband THz pulses (i.e., $\gtrsim$100 fs).

In this paper, we report the experimental observation of such a relativistic Doppler upshift in Si, using a broadband THz input pulse (obtained from a two-color gas plasma emitter [19]), with a ∼30-fs optical pump pulse and ultrabroadband detection of the reflected pulse with sum-frequency detection [20,21]. A clear signature for the Doppler upshift is observed in the measurements, which we analyze in terms of its temporal and spectral characteristics, although the magnitude of the upshift is lower than that expected based on previous predictions [10]. To reconcile the experimental observations, we also present results from one-dimensional finite-difference time-domain (1D-FDTD) simulations, which use realistic values of the effective Drude parameters at these excitation densities (in particular, with a scattering time $\tau_s \lesssim 20$ fs), and we include the influence of a weak prepulse excitation from the pump beam, which was present in the experiments here (as confirmed by auxiliary time-resolved pump-probe reflection measurements with a semi-insulating GaAs sample).

*Corresponding author: roskos@physik.uni-frankfurt.de

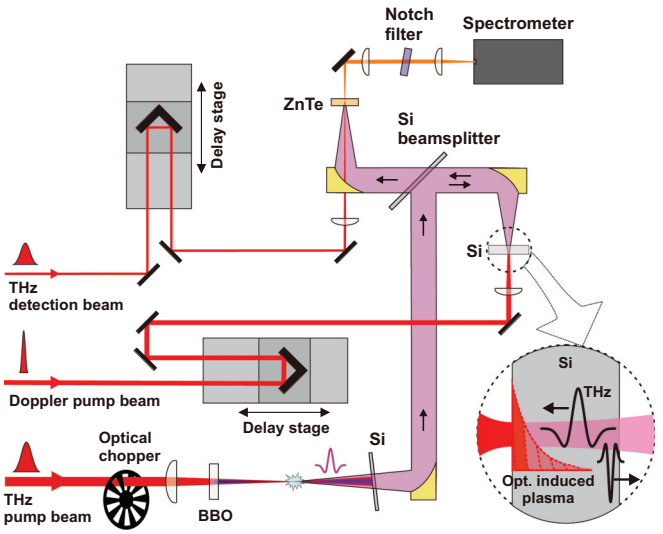

FIG. 1. (Color online) Schematic of the experimental setup, including two-color plasma-THz generation of the probe, Doppler reflection at the Si sample, and sum-frequency detection of the reflected probe pulses.

II. EXPERIMENTAL DETAILS

The experimental system (Fig. 1) is based on a 1-kHz Ti:Al_2O_3-amplifier laser with ~900 μJ pulse energy (Clark-MXR CPA-2101, $\lambda_0 = 775$ nm, $T_{FWHM} = 150$ fs), and it is comprised of an optical pump-probe setup with a normal-incidence reflection geometry for the THz probe pulse on the sample, with excitation at the back face of the Si sample with a counterpropagating pump pulse. The sample pump pulse is obtained by spectral broadening of the CPA pulses in a hollow-core fiber (HCF, filled with Ar gas at 1.7 bar) with output chirp compensation by a set of negative-dispersion mirrors [22], with a pulse width of $T_{FWHM} \sim 30$ fs at the sample (as indicated by interferometric autocorrelation measurements). The pump beam is normally incident on the sample, with a beam diameter ~2 mm achieved by using a lens with a focal length $f = 300$ mm (and placing the sample before the focal position), which leads to an excitation fluence of $F = 30\ \mu\text{J mm}^{-2}$ (accounting for Fresnel reflection losses) and a relatively homogeneous lateral profile for the THz probe beam.

The broadband THz probe beam is emitted from a two-color air plasma [19,21], whereby CPA pump pulses with ~400-μJ energy are focused with a plano-convex lens ($f = 100$ mm) via a 150-μm-thick β-BBO crystal (32°-cut) to produce the two-color plasma. The THz emission is collimated by an off-axis paraboloidal mirror (OAPM) ($f_{eff} = 152.4$ mm), before which a high-resistivity Si wafer (thickness 50 μm) is placed to discard the residual optical pump pulses. The collimated THz beam is then deflected by a high-resistivity Si beamsplitter and focused on the Si sample with a second OAPM ($f_{eff} = 101.6$ mm), where care was taken to position the THz focal plane on the backside of the sample. The reflected THz beam (including any upshifted radiation) is then recollected and transmitted through the Si beamsplitter for detection.

To measure the broadband THz pulse, we employ here optical-THz sum-frequency (SF) detection [20,21] in a 500-μm-thick ⟨110⟩-cut ZnTe crystal using 150-fs optical detection pulses (which are focused collinearly with the THz beam into the detection crystal via a central hole in the detection OAPM, $f_{eff} = 101.6$ mm). The use of a relatively thick crystal yields a smooth spectral response due to the complete loss of SF phase-matching, such that only the first coherence length of the crystal generates a net SF signal [23] (as well as a temporally separated signal from the back face of the detection crystal). Following the detection crystal, the optical beam is then recollimated and focused onto the input slit of a vis-NIR spectrometer (Ocean Optics QE65), before which a notch filter is used to discard the spectral region of the input detection pulse (which limits the frequency range here to $\gtrsim$12 THz). With this detection geometry, we can readily achieve detection of frequencies up to 150 THz (confirmed in the case of ultra-broadband plasma emission [21]), which is more than ample to detect any Doppler-upshifted spectral components in the current experiments. The SF spectra can be acquired versus detection pulse delay t to build up a full spectrogram $S(\nu,t)$, where $\nu = c(1/\lambda - 1/\lambda_0)$ is the frequency offset from the center frequency of the detection pulse.

III. RESULTS AND DISCUSSION

We first present an analysis of the THz probe beam in the absence of the sample pump. The detected signal contains various reflections occurring in the probe beam path, separated in the time domain. A summary of these is shown in Fig. 2(a)

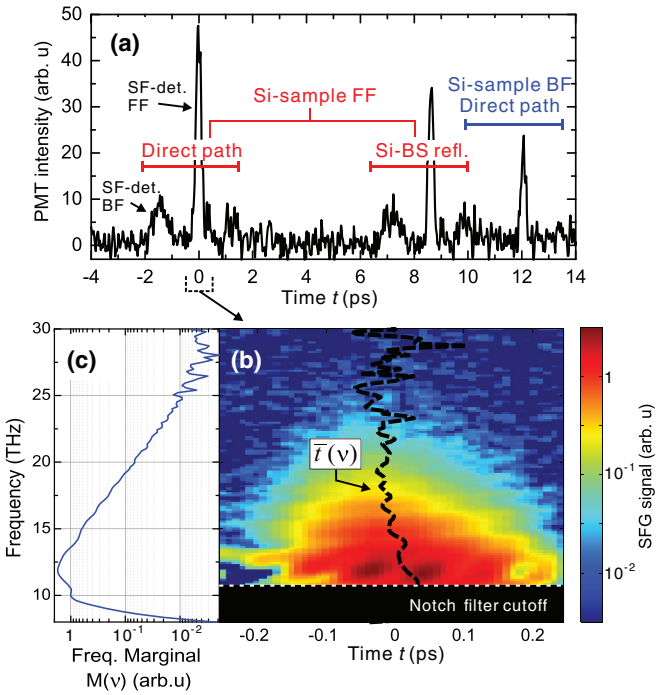

FIG. 2. (Color online) Reference measurements of THz probe pulse (without pump). (a) Spectrally integrated SF signal as a function of detection delay time t, covering both the reflected signals from the front and back face (FF, BF) of the Si sample. Primary signals (direct path) and delayed signals due to Si-beamsplitter reflections, and subcomponents due to thick-crystal SF detection as indicated (see text). (b) SF spectrogram of the THz pulse reflected from the front face of the Si sample [black curve indicates the temporal first moment $\bar{t}(\nu)$]. (c) Corresponding frequency marginal $M(\nu)$.

(spectrally integrated using a photomultiplier for detection of the SF signal). The peak at $t = 0$ ps represents the THz pulse reflected from the front face of the Si sample (passing directly through the Si beamsplitter), while the signal at $t = 8.6$ ps corresponds to this pulse with an additional double internal reflection in the Si beamsplitter (thickness 380 μm). The signal at $t = 12.1$ ps corresponds to the first detected signal due to reflection from the back face of the Si sample (thickness 525 μm), and it is relevant for the observation of pump-induced Doppler effects. Each peak is accompanied by a weaker broadened signal at a time 1.8 ps earlier due to SF generation at the back face of the detection crystal, and another weaker signal 1.2 ps later that can be assigned to the double internal reflection in the 50-μm-thick Si filter after the air plasma. In Fig. 2(b), we present a reference spectrogram $S(\nu,t)$ for the temporal region corresponding to reflection from the (unpumped) front face of the Si sample. By integrating the spectrogram signal over t, one obtains the frequency marginal spectrum $M(\nu) = \int dt\, S(\nu,t)$, as shown in Fig. 2(c), which provides a measure of the intensity spectrum of the input THz pulse, which is seen to have a measurable signal up to ~25 THz. The black curve superposed on the spectrogram represents the temporal first moment versus frequency: $\bar{t}(\nu) = \int dt\, t \cdot S(\nu,t)/M(\nu)$, which provides an estimate of the group delay $T_g(\nu)$ of the THz pulse.

For the measurement of the pump-induced changes in the THz probe pulse, we first measured the SF spectra $S(\nu,t_0;\tau)$ versus pump delay τ for a fixed SF detection time at the peak of the back-face-reflected reference signal $t = t_0 = 12.1$ ps. The array of measured spectra is shown in Fig. 3(a) (logarithmic color scale), where $\tau = 0$ corresponds to the temporal peak of the THz probe pulse arriving at the Si-sample back face coincident with the peak of the counterpropagating pump pulse. For sufficiently negative pump delay τ (before excitation), the spectra are essentially a scaled version of the reference, being due to Fresnel reflection from the Si-air interface at the back face of the sample. Around zero delay, one clearly observes the generation of a new high-frequency tail, being a direct signature of the Doppler upconversion (discussed further below). For sufficiently positive delays, where the pump pulse is fully depleted by absorption and the THz probe encounters a static plasma (with an exponential-decay spatial profile), there is a strong suppression of the reflected signal over the whole spectral range measured. This is to be expected, as based on the pump fluence one expects a plasma frequency $\omega_p/2\pi \approx 14$ THz, such that incident waves about this frequency encounter a poorly metallic (lossy) plasma and experience strong losses.

To more clearly inspect the pump-induced spectral changes, in Fig. 3(b) we plot the differential spectra $\Delta S(\nu,t_0;\tau) = S(\nu,t_0;\tau) - S(\nu,t_0;-\infty)$, where the reference $S(\nu,t_0;-\infty)$ is calculated from an average over spectra measured for sufficiently negative delay. The newly generated high-frequency tail around $\tau = 0$ is seen to extend up to ~28 THz. One can also resolve a weak positive differential feature at negative delays (in the range from ~−300 to −200 fs), followed by a partial suppression of the high-frequency components. We have identified this feature as being due to a weak satellite prepulse present in the pump beam (such that the THz

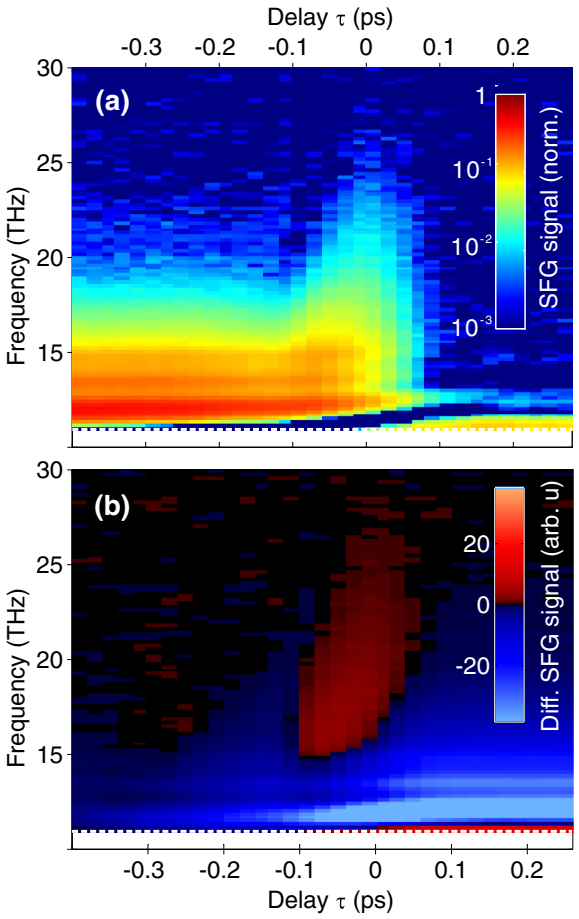

FIG. 3. (Color online) (a) Experimental SF spectra $S(\nu,t_0;\tau)$ vs pump-probe delay τ, demonstrating the reflective Doppler upshift around $\tau = 0$ (logarithmic color scale). (b) Corresponding differential SF spectra $\Delta S(\nu,t_0;\tau)$ (obtained by subtracting the SF spectrum for sufficiently negative delay).

probe encounters a preexisting, underdense plasma profile at these values of delay), and we discuss its impact on these experiments below.

While the acquisition of the spectra $S(\nu,t_0;\tau)$ at constant detection time t (with a 150-fs detection gate pulse) is a practical method to obtain an overview of the pump-induced effects versus delay, one must consider that as the plasma profile penetrates into the Si medium (with an absorption depth $1/\alpha_{ex} = 8$ μm for $\lambda_{ex} = 775$ nm), part of the reflected probe may well be detected at an earlier time t. Hence we also measured full spectrograms $S(\nu,t;\tau_n)$ at selected pump-probe delays τ_n, as shown in Figs. 4(a)–4(d) (with $\tau_n = -1.0$, -0.15, 0, and 0.05 ps, respectively), which allows one to calculate spectral marginals $M(\nu)$ over a sufficient range to capture any temporally shifted signal, as well as to analyze such shifts via $\bar{t}(\nu)$. The corresponding marginal spectra $M(\nu)$ and temporal first-moment change $\Delta\bar{t}(\nu)$ [the latter relative to $\bar{t}(\nu)$ for $\tau = -1.0$ ps] for each τ_n are shown in Figs. 4(e) and 4(f), respectively.

Considering first the delay value $\tau_n = -0.15$ ps [i.e., before the main excitation pulse, but after the prepulse feature in Fig. 3(b)], as can be seen by comparing $M(\nu)$ with that for $\tau_n = -1.0$ ps, there is a reduction in the reflected THz

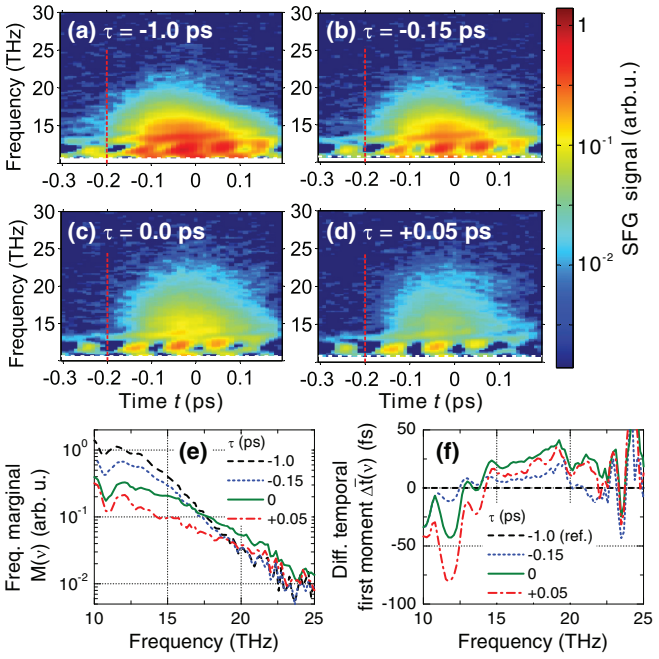

FIG. 4. (Color online) Detected spectrograms $S(\nu,t;\tau_n)$ for selected pump-probe delays τ_n: (a) -1.0 ps, (b) -0.15 ps, (c) 0 ps, (d) $+0.05$ ps. Vertical dashed curves at $t = -0.2$ ps added to aid comparison of the temporal rising edge of each spectrogram (see text). (e) Corresponding frequency marginals $M(\nu)$ and (f) relative temporal first-moment $\Delta\bar{t}(\nu)$.

spectrum, by a factor that is largest at low frequencies and progressively disappears in going to higher frequencies. The relative group delay is slightly negative (i.e., detected earlier) for frequencies below ∼13 THz, above which it grows to become slightly positive. These trends are consistent with the reflection from a preformed low-density plasma profile: For the lower-frequency range measured, the plasma has the character of a poor metal, leading to absorption of the radiation which penetrates toward the Si-air interface, and a partial reflection from the plasma density gradient in the Si medium results in an earlier mean arrival time at the detector. At higher frequencies, the preformed plasma properties approach that of a dielectric (with only a small index change relative to the background Si medium n_b), such that the radiation can reach (and reflect from) the Si-air interface with only minor losses and a positive group delay due to the positive *group* dispersion of a plasma for $\omega \gg \omega_p$: $n_g \approx n_b + \omega_p^2/2\omega^2$.

For $\tau_n = 0$, the low-frequency range is further suppressed and the newly generated frequency components due to the Doppler upconversion can be observed in the high-frequency tail. While the more negative group delay of the low-frequency range is consistent with partial reflection from the dense plasma profile, which has penetrated into the Si medium, the further increase of the positive group delay for the frequency range from ∼15 to 20 THz may at first be unexpected, as the plasma medium here should now be poorly metallic (i.e., lossy for any reflection at the Si-air interface) and one expects that a significant fraction of this radiation is due to Doppler upconversion of lower incident frequency components from the plasma front inside the Si medium. This issue can be resolved by closer inspection of the spectrograms in Figs. 4(a)–4(d), in particular the rising temporal edge at negative t (vertical dashed lines are added to aid visual comparison). As can been seen, this edge—which is due to detection of the leading edge of the THz probe pulse—progressively shifts to more positive t with increasing τ (in particular, for the spectral range from 15 to 20 THz). Hence the positive group delay is predominantly due to a suppression of these frequencies in the incident leading edge of the pulse, which interacts with a lower-density, lossy plasma medium during the initial propagation of the pump pulse. This positive group-delay shift then decays in the frequency range above 20 THz—this is to be expected, as here the signal should be dominated by the newly formed Doppler-upshifted signal (i.e., there is no significant input leading edge at these frequencies to suppress). For $\tau = +0.05$ ps, the high-frequency tail has decayed significantly, demonstrating that the delay-time window for the upconversion is on the order of 100 fs, consistent with the fixed-time spectra $S(\nu,t_0,\tau)$ in Fig. 3 (i.e., the observation of the Doppler upconversion there is not significantly distorted due to the use of a fixed detection time t_0).

To further investigate the presence of a weak prepulse in the pump beam, we carried out additional optical-pump THz-probe measurements. In this case, we used a conventional reflection geometry with front-face excitation (also using optical pulses from the HCF compressor, with a somewhat shorter duration of ∼20 fs), and a THz-midinfrared continuum from a two-color gas plasma as the probe pulse with a bandwidth of ∼150 THz [21,22] and SF detection. We chose semi-insulating GaAs as the sample due to its significantly higher absorption coefficient ($\alpha_{ex} = 1.5\ \mu m^{-1}$) [24] for the optical pump beam (and hence higher front-face plasma density), which makes it highly sensitive to any weak prepulse features. The relative reflectivity spectra $R'(\nu,t_0;\tau)$ (i.e., normalized to the intensity reflection of the unpumped sample) versus pump-probe delay τ are shown in Fig. 5. At $\tau = 0$, as the main peak of the pump

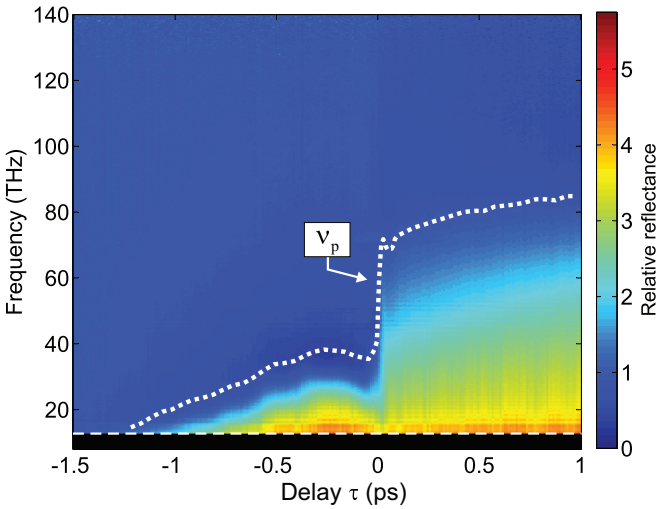

FIG. 5. (Color online) Relative reflectivity spectra $R'(\nu,t_0;\tau) = R(\nu,t_0;\tau)/R_0(\nu,t_0)$ vs pump delay τ of GaAs sample in a front-face optical-pump THz-mid-ir-probe experiment. Drude plasma frequency $\nu_p = \omega_p/2\pi$ from fitting each spectrum vs τ included as a dotted curve.

pulse arrives at the sample, one observes a sharp increase in the plasma frequency (corresponding to $\omega_p/2\pi \sim 72$ THz, as determined from fitting each spectrum with a Drude model and accounting for the depth profile of the excitation [25,26]). However, one can also clearly observe a signature starting from about $\tau = -1$ ps with a maximum spectral extension at $\tau = -250$ fs, due to a prepulse feature in the pump beam. From the simple Drude analysis, the response at $\tau = -250$ fs suggests an excitation density of ~25–30% compared to the main peak at $\tau = 0$. An additional gradual rise in the plasma frequency for $\tau > 0$ also suggests significant energy following the main pulse peak. The presence of such a satellite temporal structure in our experiments appears to be related to the use of self-phase modulation to achieve the required optical bandwidth of the pump pulses in the HCF (resulting in a strongly modulated intensity spectrum), in conjunction with residual higher-order dispersion. We note that these measurements on GaAs employed a larger spectral broadening in the HCF than was used for the Doppler experiments above, such that the amplitude of such features should be lower for the Doppler results. Nevertheless, it is reasonable to assume that the relative pump prepulse energy was at least well into the percent level in those experiments as well. (We note that the partial recovery of the spectral response between $\tau = -200$ and 0 fs indicates that the response is not simply based on the cumulative pump fluence on the sample, which we believe is due to initial carrier dynamics in the GaAs sample and is currently under further investigation.)

In a previous report, we presented results based on 1D-FDTD simulations [10] for the expected Doppler upshift in experiments similar to those presented here, which indicated that a significant upshift could be achieved (with components approaching even 100 THz with a sufficiently short pump pulse), assuming a Drude scattering time of $\tau_s = 50$–250 fs. However, we have recently carried out experiments on the Drude response of photoexcited Si in the relevant excitation density range ($N_{ex} \sim 10^{19}$ cm^{-3}) [26], which indicate that the effective scattering time scale is much shorter, i.e., in the range $\tau_s = 20$–30 fs and possibly as short as 15 fs during initial subpicosecond relaxation. This increases the negative impact of the leading tail of the plasma front (as the density/frequency range corresponding to poor metallic behavior is broadened with decreasing τ_s), although simulations show that this can be reduced through the use of a shorter pump pulses. Here we present simulations using such a reduced value of τ_s, as well as accounting for the impact of a prepulse feature in the pump beam, as suggested by the experimental data. The implementation of the FDTD algorithm is as in Ref. [10], here with a pump-pulse duration $T_{FWHM} = 30$ fs and fluence $F = 30$ μJ mm^{-2} (with an absorption coefficient of $\alpha_{ex} = 125$ mm^{-1} at $\lambda_{ex} = 775$ nm yielding an excitation density of $N_{ex} = 1.5\times10^{19}$ cm^{-3}), and taking $\tau_s = 15$ fs as a conservative lower value to avoid overestimating the predicted performance of the Doppler effect. An additional prepulse, with a relative pulse energy of $\eta = 5\%$ and duration 200 fs, is optionally added in the simulations at $t_{pp} = -250$ fs (this value of η was chosen after preliminary simulations, as it yielded the best qualitative correspondence to the experimental results). The input THz pulse is generated by using a multiple-Gaussian intensity spectrum (with no temporal chirp) in

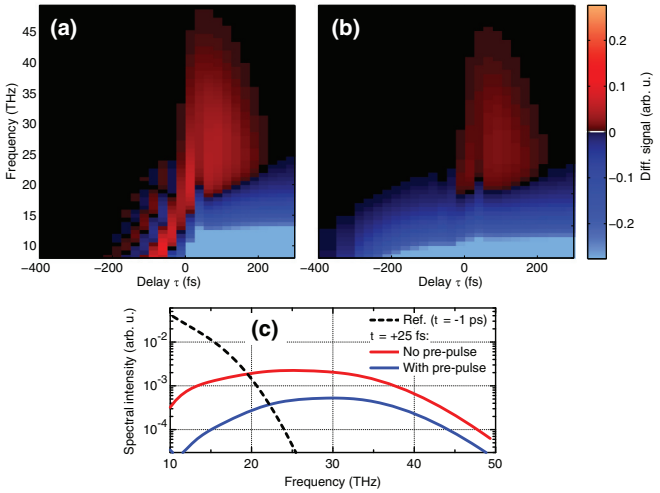

FIG. 6. (Color online) Predicted differential spectra $\Delta S(\nu,t_0;\tau)$ vs pump delay τ from 1D-FDTD simulations: (a) without and (b) with additional prepulse at $t_{pp} = -250$ fs (see text for parameters). (c) Comparison of spectra $\Delta S(\nu,t_0;\tau)$ for $\tau = 25$ fs (maximum Doppler upshift), including a reference spectrum (at sufficiently negative delay, $\tau = -1$ ps, i.e., corresponding to linear reflection from the Si-air interface).

order to reproduce the experimental spectrum [i.e., the full spectrum as measured by Fourier transform infrared (FTIR) detection [21] as well as the high-frequency tail as shown above in Fig. 2(c)]. Simulation batches versus the pump-probe delay τ were carried out to build up an array of reflected THz spectra, as per the experimental results in Fig. 3 (using a 150-fs Gaussian temporal gate on the numerical THz field to reproduce the effect of SF detection at constant t).

The results are shown in Figs. 6(a) and 6(b), for the cases with and without the prepulse, respectively, where we plot the differential data $\Delta S(\nu,t_0;\tau)$, as per the experimental data in Fig. 3(b), to aid comparison. Absolute intensity spectra $S(\nu,t_0;\tau)$ are also shown in Fig. 6(c) for $\tau = 25$ fs (which corresponded to the maximum upshift in the simulations), including a reference spectrum for sufficiently negative delay (i.e., arising from Fresnel reflection from the Si-air interface). For the case without a prepulse, the simulations predict that upshifted components reaching ~50 THz should be generated in the reflected THz pulse. The spectral/temporal oscillations in the data in Fig. 6(a) around $\tau = 0$ arise due to the interference between waves reflected from the plasma front and Si-air interface [10]. The addition of the prepulse leads to a negative differential signal at negative τ as well as a suppression of the upshifted energy for positive delays due to the presence of the lossy preformed plasma profile (as discussed above for the experimental data). The suppression factor is over an order of magnitude in the lower-frequency range shown, reducing to a factor of ~2.5 in the high-frequency range.

While this demonstrates that even such a relatively weak pump prepulse is expected to cause significant losses for the upshifted radiation, the simulations still predict a significantly stronger Doppler effect than that measured experimentally (Fig. 3), even when considering the possible role of the detection noise floor (recall that the nominal SF detection

bandwidth is well above 100 THz). Several reasons may account for this discrepancy, which we address in turn. First, the 1D-FDTD simulations imply plane waves for both THz and optical pump beams. It is possible that the high-frequency upshifted radiation suffers diffraction effects due to the lateral gradient of the pump beam profile and is not efficiently imaged to the SF detector crystal. We note that control measurements were made by shifting the longitudinal position of the SF crystal to check if any defocusing effects occur in the Si sample due to the pump beam profile. In the experiments here, the use of a larger pump beam did not improve the strength of the Doppler signal due to the concomitant loss of fluence. Secondly, due to the high sensitivity of the Doppler process to the leading edge of the pump pulse, a more rigorous characterization of its precise temporal intensity profile, including any possible lateral spatial dependence [27], needs to be performed in future experiments. Thirdly, the assumption of a simple Drude response for the plasma in the FDTD simulations should be investigated further using advanced nonequilibrium theory for the charge-carrier dynamics [28], especially considering that it is the plasma directly following excitation that plays the key role in the ionization front.

IV. CONCLUSION

We have demonstrated experimentally the relativistic Doppler reflection from a photoinduced charge-carrier plasma front in Si for incident THz pulses. The presence of a weak prepulse energy in the pump pulse was demonstrated and shown to have a strong effect on the process. Simulations using revised values for the Drude scattering time ($\lesssim$20 fs) still predict that a significant upshift—sufficient to be of practical use for enhancing the bandwidth coverage of existing THz sources—should be achievable. Considering future directions for experimental investigation of the reflective Doppler effect, one avenue is to employ other semiconductor media such as GaAs. Here the considerably higher absorption coefficient for pump wavelengths $\lambda_{ex} \sim 800$ nm ($\alpha_{ex} = 1.5\ \mu m^{-1}$ compared to 0.13 μm^{-1} for Si [24]) would allow for higher excitation densities over a larger cross section, although at the cost of a shorter interaction time t_α (over which the pump is depleted). The ability to suppress/steepen the leading edge of the pump pulse is predicted to enhance the Doppler upshift effect significantly, such that one could consider the use of a saturable absorber medium [29] and/or careful control and optimization of the pump spectral shape and dispersion. Also, the use of multiphoton excitation would provide an effective means to achieve a very clean and steep temporal plasma front. One option would be to use two-photon absorption in solid-state media (in particular, with a fundamental pump photon energy below the band gap), although in typical semiconductors, the required fluence to reach excitation densities in the range $N_{ex} = 10^{18}$–10^{19} cm^{-3} may cause damage to the medium or induce additional higher-order nonlinear effects. The use of tunnel ionization in gaseous media, as proposed previously [11], is an interesting option—however, to achieve the required density and lateral cross section ($\sim$1 mm^2) for focused input THz beams would require a large-scale laser amplifier system with pulse energies well above 10 mJ. Hence, the solid-state charge-carrier plasmas, as presented here (where sub-mJ pump pulse energies are sufficient), are much more readily accessible for table-top-scale experiments with kHz-amplifier lasers.

ACKNOWLEDGMENT

We gratefully acknowledge financial support from the Deutsche Forschungsgemeinschaft (DFG) for this research work.

[1] W. Pauli, *Theory of Relativity* (Pergamon, New York, 1958).
[2] V. L. Granatstein, P. Sprangle, R. K. Parker, J. Pasour, M. Herndon, and S. P. Schlesinger, Phys. Rev. A **14**, 1194 (1976).
[3] T. Dewandre, J. R. Albritton, and E. A. Williams, Phys. Fluids **24**, 528 (1981).
[4] S. V. Bulanov, T. Esirkepov, and T. Tajima, Phys. Rev. Lett. **91**, 085001 (2003).
[5] M. Kando, Y. Fukuda, A. S. Pirozhkov, J. Ma, I. Daito, L.-M. Chen, T. Z. Esirkepov, K. Ogura, T. Homma, Y. Hayashi, H. Kotaki, A. Sagisaka, M. Mori, J. K. Koga, H. Daido, S. V. Bulanov, T. Kimura, Y. Kato, and T. Tajima, Phys. Rev. Lett. **99**, 135001 (2007).
[6] M. Kando, A. S. Pirozhkov, K. Kawase, T. Z. Esirkepov, Y. Fukuda, H. Kiriyama, H. Okada, I. Daido, T. Kameshima, Y. Hayashi, H. Kotaki, M. Mori, J. K. Koga, H. Daido, A. Y. Faenov, T. Pikuz, J. Ma, L.-M. Chen, E. N. Ragozin, T. Kawachi, Y. Kato, T. Tjima, and S. V. Bulanov, Phys. Rev. Lett. **103**, 235003 (2009).
[7] D. Kiefer, M. Yeung, T. Dzelzainis, P. S. Foster, S. G. Rykovanov, C. L. S. Lewis, R. S. Marjoribanks, H. Ruhl, D. Habs, J. Schreiber, M. Zepf, and B. Dromey, Nat. Commun. **4**, 1763 (2013).
[8] V. I. Semenova, Izv. Vyssh. Uchebn. Zaved., Radiofiz. **10**, 1077 (1967) [Radiophys. Quantum Electron. **10**, 599 (1967)].
[9] E. O. M. Lampe and J. Walker, Phys. Fluids **21**, 42 (1978).
[10] M. D. Thomson, S. M. Tzanova, and H. G. Roskos, Phys. Rev. B **87**, 085203 (2013).
[11] H. C. Kapteyn and M. M. Murnane, J. Opt. Soc. Am. B **8**, 1657 (1991).
[12] M. C. Hoffman and J. A. Fulop, J. Phys. D **44**, 083001 (2011).
[13] H. Hirori, A. Doi, F. Blanchard, and K. Tanaka, Appl. Phys. Lett. **98**, 091106 (2011).
[14] K. L. Yeh, M. C. Hoffman, J. Hebling, and K. Nelson, Appl. Phys. Lett. **90**, 171121 (2007).
[15] A. Dreyhaupt, S. Winnerl, T. Dekorsy, and M. Helm, Appl. Phys. Lett. **86**, 121114 (2005).
[16] M. Tsubouchi, M. Nagai, and Y. Ohshima, Opt. Lett. **37**, 3528 (2012).
[17] A. Schuelzgen, N. Peyghambarian, and S. Hughes, Phys. Status Solidi **206**, 125 (1998).
[18] W. Forysiak, R. G. Flesch, J. V. Moloney, and E. M. Wright, Phys. Rev. Lett. **76**, 3695 (1996).
[19] M. D. Thomson, M. Kreß, T. Löffler, and H. G. Roskos, Laser Photon. Rev. **1**, 349 (2007).

[20] M. D. Thomson, V. Blank, and H. G. Roskos, Eur. Phys. J. Web Conf. **41**, 09011 (2013).
[21] V. Blank, M. D. Thomson, and H. G. Roskos, New J. Phys. **15**, 075023 (2013).
[22] M. D. Thomson, V. Blank, and H. G. Roskos, Opt. Express **18**, 23173 (2010).
[23] T. Kampfrath, J. Nötzold, and M. Wolf, Appl. Phys. Lett. **90**, 231113 (2007).
[24] E. D. Palik, *Handbook of Optical Constants of Solids* (Academic, New York, 1985).
[25] J. Y. Vinet, M. Combescot, and C. Tanguy, Solid State Commun. **51**, 171 (1984).
[26] F. Meng, M. D. Thomson, B. E. Sernelius, M. Jörger, and H. G. Roskos (unpublished).
[27] F. Eilenberger, A. Brown, S. Minardi, and T. Pertsch, Opt. Express **21**, 25968 (2013).
[28] R. Binder and S. Koch, Prog. Quantum Electron. **19**, 307 (1995).
[29] K.-H. Hong, B. Hou, J. A. Nees, E. Power, and G. A. Mourou, Appl. Phys. B **81**, 447 (2005).